Control design for an octorotor for radar applications

Maria Makarov, Cristina Stoica Maniu, Sihem Tebbani, Israel Hinostroza

Control Design for an Octorotor for Radar Applications

Maria Makarov, Cristina Stoica Maniu and Sihem Tebbani
Laboratoire des Signaux et Systèmes
CentraleSupélec-CNRS-Univ. Paris-Sud, Université Paris-Saclay,
France, Gif-sur-Yvette F91192
E-mail: {maria.makarov; cristina.stoica; sihem.tebbani}@centralesupelec.fr

Israel Hinostroza
SONDRA Lab
CentraleSupélec
France, Gif-sur-Yvette F91192
E-mail: israel.hinostroza@supelec.fr

***Abstract*—As part of a research and educational project, this paper proposes an H_∞ controller for an octorotor used for radar applications. In the context of a vertical take-off and landing multirotor with an embedded radar system, the H_∞ controller synthesis is developed based on a simplified linearized model and tested in simulation on the nonlinear model. A wind model, including turbulence and gust wind, has been considered in order to validate the robustness of the proposed controller.**

I. Introduction

In the last few years, the possibility to use small UAVs as platforms for radars has been substantially investigated [1], [2]. The objective of the present research and educational project is to design a VTOL (vertical take-off and landing) multirotor with an embedded radar system for civilian applications like crop field monitoring, damage evaluation after natural disasters, rescue operations after avalanches etc. In this context, a critical point that will affect the collected data is a stabilized attitude of the flying platform and its ability to precisely follow a prescribed trajectory, despite the possible wind disturbances.

A commercially available octorotor (ARF-MikroKopter OktoXL, Mikrokopter, HiSystems GMBH) [3], [4] compatible with the required radar payload and the redundancy provided by the eight rotors, is considered in this paper. To meet the requirements of radar applications, the control system has to guarantee an efficient trajectory tracking, at a constant and relatively high speed [5], in spite of possible external wind disturbances [6]. Recently, various control schemes for attitude control or trajectory tracking have been presented for quadrotors [7], hexarotors [8] and octorotors [9], [10]. Among the linear control methods (see for example [11], [12] for reviews on the main control methods of multirotors), H_∞ control design methods are well adapted to solve the posed multivariable control problem with competing specifications on performance and robustness. The latter are especially important in presence of uncertainties [13] or external disturbances.

Using the model proposed in [5], this paper focuses on the H_∞ control design of the octorotor ARF-MikroKopter OktoXL. In order to increase the robustness of the controlled system, a keypoint consists in considering wind disturbances directly in the controller synthesis step. The octorotor with the thus designed multivariable controller is able to follow a reference trajectory specified in terms of positions in space and the yaw angle. The inputs to the designed multivariable controller are the octorotor positions and attitude angles, and its outputs are the eight motors rotational speeds.

Section II is dedicated to the octorotor model analysis and the desired control specifications in view of radar applications. The H_∞ control design is presented in Section III. The proposed control law is validated through simulation results illustrated in Section IV. Finally, concluding remarks are drawn in Section V.

II. System description and control specifications

The considered multirotor (Figure 1) has eight brushless motors with twin-bladed propellers, arranged in a star-shaped way. Longer arms of length L correspond to odd-numbered motors (providing higher torques) which rotate in the clockwise direction, whereas shorter arms of length l correspond to even-numbered motors (providing less momentum) which rotate in the oposite direction. Thus, this configuration improves the handling ability of the drone. Choosing opposite directions of rotation between the odd- and even-numbered motors is the solution to compensate the drag torque. The motors are fixed with a 3° inclination with respect to the vertical axis Z. The drone main parameters are provided in Table I.

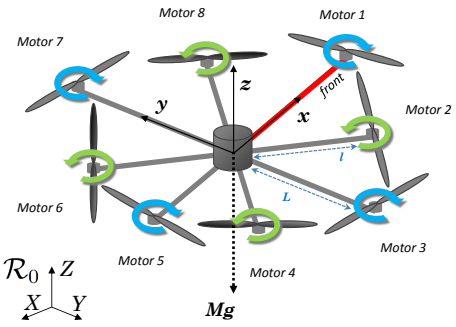

Figure 1: Considered octorotor and reference frames.

A. Control requirements for radar applications

Synthetic Aperture Radar (SAR) image formation is based on the coherent sum of the scattered waves due to the periodic illumination of a scene by the radar [14]. For stripmap mode, sideway illumination (relative to the UAV movement) of the

Table I: Drone parameters: notation and value (units).

Mass of 1 motor	m_m = 0.1 (kg)
Mass of 1 battery	m_b = 0.534 (kg)
Mass of central block	m_c = 1.226 (kg)
Total mass with 1 battery	m = 2.56 (kg)
Motor radius, height	r_m = 0.0175, h_m = 0.038 (m)
Central block radius, height	r_c = 0.09, h_c = 0.095 (m)
Battery width, length, height	w_c = 0.132, l_c = 0.09, h_c = 0.02 (m)
Arm lengths (short, long)	L = 0.455, l = 0.349 (m)

scene with constant inclination, altitude, speed and linear trajectory, is desired. Both the radar specifications for the X band FM Continuous Wave SAR and the control specifications to be used are summarized in Table II.

Table II: Requirements for radar applications.

Radar specifications	- Platform speed	10 m/s
	- Ground resolution	0.8x1 m
	- Height of flight	100 m
	- Ground range	250 - 550 m
Control specifications	- Translation speed	10 m/s $\pm$ 0.2 m/s
	- Maximum trajectory deviation	less than 1 m
	- Operational altitude	100 m
	- Stabilized attitude	

B. System description

The nonlinear equations of motion in the state-space form are written using the following state vector: $\boldsymbol{X} = [X \;\; Y \;\; Z \;\; \varphi \;\; \theta \;\; \psi \;\; V_x \;\; V_y \;\; V_z \;\; \omega_x \;\; \omega_y \;\; \omega_z]^T$ where X, Y, Z are the position of the drone in the Earth's frame, and V_x, V_y, V_z their time derivatives, φ, θ, ψ the Euler angles defining the orientation of the drone in the Earth's frame, and $\omega_x, \omega_y, \omega_z$ the angular speeds of the drone expressed in its own frame.

The complete nonlinear model [5] describing the dynamics of the drone is further used:

$$\dot{X} = V_x, \quad \dot{Y} = V_y, \quad \dot{Z} = V_z \tag{1}$$

$$\dot{\varphi} = \omega_x + s\varphi \frac{s\theta}{c\theta}\, \omega_y + c\varphi \frac{s\theta}{c\theta}\, \omega_z \tag{2}$$

$$\dot{\theta} = c\varphi\, \omega_y - s\varphi\, \omega_z \tag{3}$$

$$\dot{\psi} = \frac{s\varphi}{c\theta}\, \omega_y + \frac{c\varphi}{c\theta}\, \omega_z \tag{4}$$

$$\begin{aligned} m\dot{V}_x = {} & (c\psi c\theta)F_x^R + (c\psi s\theta s\varphi - s\psi c\varphi)F_y^R \\ & + (c\psi s\theta c\varphi + s\psi s\varphi)F_z^R + F_x^{air} \end{aligned} \tag{5}$$

$$\begin{aligned} m\dot{V}_y = {} & (s\psi c\theta)F_x^R + (s\psi s\theta s\varphi + c\psi c\varphi)F_y^R \\ & + (s\psi s\theta c\varphi - c\psi s\varphi)F_z^R + F_y^{air} \end{aligned} \tag{6}$$

$$\begin{aligned} m\dot{V}_z = {} & (-s\theta)F_x^R + (c\theta s\varphi)F_y^R + (c\theta c\varphi)F_z^R \\ & + F_z^{air} - mg \end{aligned} \tag{7}$$

$$I_{xx}\dot{\omega}_x = (I_{yy} - I_{zz})\omega_y\omega_z + \tau_x^R \tag{8}$$

$$I_{yy}\dot{\omega}_y = (I_{zz} - I_{xx})\omega_x\omega_z + \tau_y^R \tag{9}$$

$$I_{zz}\dot{\omega}_z = (I_{xx} - I_{yy})\omega_x\omega_y + \tau_z^R \tag{10}$$

The symbols $I_\square$, $F_\square^R$, $\tau_\square^R$ and $F_\square^{air}$ represent resp. the inertia components, the resulting propeller force, the torque and the air drag force in the specified direction (variables expressed in the drone's frame are denoted by the superscript R). Here, $s\square$ and $c\square$ mean resp. $sin(\square)$ and $cos(\square)$. The thrust force and drag torque generated by the i-th propeller are assumed to be proportional to the squared propeller's speed Ω_i. This model has thus eight inputs (rotational speed of each motor Ω_i) entering the equations through $F_\square^R$and $\tau_\square^R$. The air drag effects are assumed to be proportional to the square of the speed of the object relative to the air . A linearized model[1] around the origin (i.e. null velocities, null Euler angles, null rotational velocities) will be used for the H_∞ controller synthesis.

III. Controller design

The inputs and outputs of the considered problem formulation under the Linear Fractional Transformation (LFT) form are illustrated in Figure 2. Here $\boldsymbol{P}$ denotes the octorotor linearized model, suitably augmented for the H_∞ design, and $\boldsymbol{K}$ denotes the controller. The external inputs to the augmented system are regrouped in $\boldsymbol{w}$, and the controlled outputs are represented by $\boldsymbol{z}$. The inputs and outputs to the controller are respectively denoted $\boldsymbol{y}$ and $\boldsymbol{u}$.

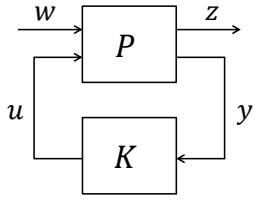

Figure 2: LFT form.

The H_∞ control problem is then formulated as follows:

$$\begin{aligned} & \min \gamma \\ & \text{s.t.} \left\| LFT(\boldsymbol{P}, \boldsymbol{K}) \right\|_\infty < \gamma \end{aligned} \tag{11}$$

For the controller design step, the structure of the augmented system $\boldsymbol{P}$ is detailed in Figure 3. The blocs $\boldsymbol{W}_1, \boldsymbol{W}_2, \boldsymbol{W}_3, \boldsymbol{W}_4$ and $\boldsymbol{W}_5$ are the design parameters and correspond to filters that allow us to shape the closed-loop response between the selected inputs and outputs according to the specifications. The signals $\boldsymbol{w}, \boldsymbol{z}, \boldsymbol{y}$ and $\boldsymbol{u}$ are explained below.

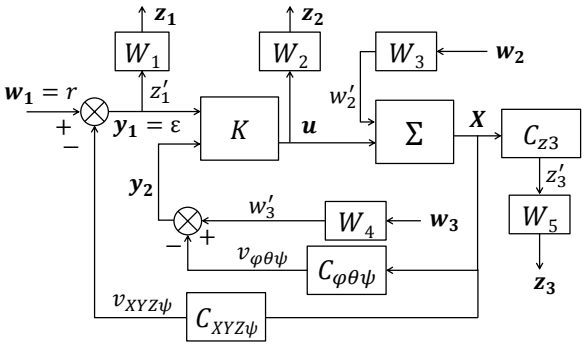

Figure 3: Augmented system with controller $\boldsymbol{K}$ for H_∞ control design.

[1]The linearization details can be found in [5].

The external inputs $\boldsymbol{w} = \begin{bmatrix}\boldsymbol{w}_1^T & \boldsymbol{w}_2^T & \boldsymbol{w}_3^T\end{bmatrix}^T$ contain the desired reference trajectories $\boldsymbol{w}_1 = \begin{bmatrix}r_X & r_Y & r_Z & r_\psi\end{bmatrix}^T \in \mathbb{R}^4$ to be followed by the variables X, Y, Z, ψ, the disturbances $\boldsymbol{w}_2 \in \mathbb{R}^3$ due to the wind and modeled as disturbances on the drone's velocities V_x, V_y, V_z, and the additional inputs $\boldsymbol{w}_3 \in \mathbb{R}^3$ used in the control design.

The controlled outputs $\boldsymbol{z} = \begin{bmatrix}\boldsymbol{z}_1^T & \boldsymbol{z}_2^T & \boldsymbol{z}_3^T\end{bmatrix}^T$ represent the filtered versions by respectively $\boldsymbol{W}_1, \boldsymbol{W}_2, \boldsymbol{W}_5$ of the following signals: the errors $\boldsymbol{\varepsilon} \in \mathbb{R}^4$ on X, Y, Z, ψ with respect to the references, the control inputs $\boldsymbol{u} \in \mathbb{R}^8$, and the additional controlled outputs $\boldsymbol{z}_3' = \begin{bmatrix}\varphi & \theta & V_x & V_y & \omega_x\end{bmatrix}^T$ used in the control design to emphasize their stabilization.

The controller inputs $\boldsymbol{y} = \begin{bmatrix}\boldsymbol{y}_1^T & \boldsymbol{y}_2^T\end{bmatrix}^T$ contain the errors $\boldsymbol{y}_1 = \boldsymbol{\varepsilon}$ and the additional inputs $\boldsymbol{y}_2 = -\boldsymbol{v}_{\varphi\theta\psi} = -\begin{bmatrix}\varphi & \theta & \psi\end{bmatrix}^T$ which are affected by additional fictitious inputs $\boldsymbol{w}_3'$ during the design phase. The controller outputs $\boldsymbol{u} = \begin{bmatrix}\Omega_1 & \Omega_2 & \Omega_3 & \Omega_4 & \Omega_5 & \Omega_6 & \Omega_7 & \Omega_8\end{bmatrix}^T \in \mathbb{R}^8$ are the motor rotation speeds.

According to these notations and to the control design structure summarized in Figure 3, the closed-loop transfer matrix between the external inputs $\boldsymbol{w}$ and controlled outputs $\boldsymbol{z}$ in the H_∞ problem (11) is expressed as follows:

$$\boldsymbol{z} = LFT(\boldsymbol{P}, \boldsymbol{K})\boldsymbol{w} \tag{12}$$

$$\begin{bmatrix}\boldsymbol{z}_1\\ \boldsymbol{z}_2\\ \boldsymbol{z}_3\end{bmatrix} = \begin{bmatrix}\boldsymbol{W}_1\boldsymbol{T}_{r\to\varepsilon} & \boldsymbol{W}_1\boldsymbol{T}_{w_2'\to\varepsilon}\boldsymbol{W}_3 & \boldsymbol{W}_1\boldsymbol{T}_{w_3'\to\varepsilon}\boldsymbol{W}_4\\ \boldsymbol{W}_2\boldsymbol{T}_{r\to u} & \boldsymbol{W}_2\boldsymbol{T}_{w_2'\to u}\boldsymbol{W}_3 & \boldsymbol{W}_2\boldsymbol{T}_{w_3'\to u}\boldsymbol{W}_4\\ \boldsymbol{W}_5\boldsymbol{T}_{r\to z_3'} & \boldsymbol{W}_5\boldsymbol{T}_{w_2'\to z_3'}\boldsymbol{W}_3 & \boldsymbol{W}_2\boldsymbol{T}_{w_3'\to z_3'}\boldsymbol{W}_4\end{bmatrix}\begin{bmatrix}\boldsymbol{w}_1\\ \boldsymbol{w}_2\\ \boldsymbol{w}_3\end{bmatrix}$$

where $\boldsymbol{T}_{a\to b}$ denotes the transfer matrix from the input a to the output b.

The weighting functions $\boldsymbol{W}_1, \boldsymbol{W}_2, \boldsymbol{W}_3, \boldsymbol{W}_4, \boldsymbol{W}_5$ are used as the tuning parameters in the proposed design. As in a classical four-block H_∞ control design, $\boldsymbol{W}_1, \boldsymbol{W}_2, \boldsymbol{W}_3$ are used to shape respectively the sensitivity function $\boldsymbol{S} \overset{def}{=} \boldsymbol{T}_{r\to\varepsilon}$ (which influences the response to the reference), the transfer $\boldsymbol{KS} \overset{def}{=} \boldsymbol{T}_{r\to u}$ (which influences the control signal) and the transfer $\boldsymbol{SG} \overset{def}{=} \boldsymbol{T}_{w_2'\to\varepsilon}$ (which influences the response to the disturbances). Once $\boldsymbol{W}_1, \boldsymbol{W}_2, \boldsymbol{W}_3$ are fixed, the weighting on the transfer $\boldsymbol{KSG} \overset{def}{=} \boldsymbol{T}_{w_2'\to u}$ is fixed too. Moreover, $\boldsymbol{W}_4$ is used to tune the influence of the input $\boldsymbol{v}_{\varphi\theta\psi}$ with respect to $\boldsymbol{y}_1$ in the controller. Finally, $\boldsymbol{W}_5$ is used to weight the importance of the additional controlled outputs $\boldsymbol{z}_3'$.

The weighting functions $\boldsymbol{W}_1, \boldsymbol{W}_2, \boldsymbol{W}_3$ are chosen as first order filters with stable inverses and are represented in Figure 4. $\boldsymbol{W}_4$ and $\boldsymbol{W}_5$ are fixed to 1. The design problem is solved by Linear Matrix Inequalities (LMI) method using Matlab `hinfsyn` function. The obtained controller is of order 25, and has 7 inputs and 8 outputs. The maximum singular values of the corresponding closed-loop transfer matrices with the obtained controller ($\gamma = 3$) are represented in Figure 4 and fulfill the specifications.

IV. Simulation Results

The previously designed controller has been reduced to the order 15, and then evaluated in simulation with the complete nonlinear model. The simulation corresponds to the case study for radar applications described in Section II-A.

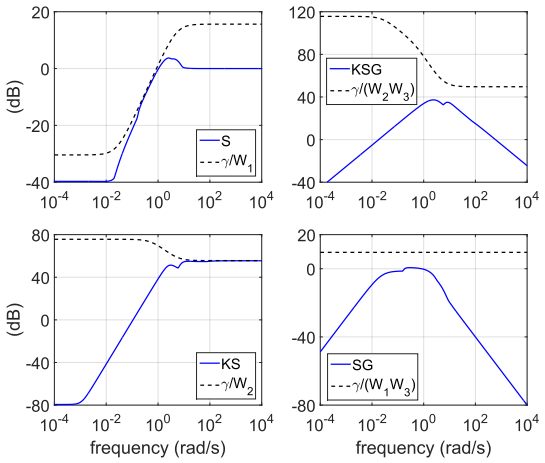

Figure 4: Maximum singular values of closed-loop transfer matrices and corresponding weighting functions.

The trajectory reference corresponds first to a take-off until an altitude of 100 m is reached, followed by a translation on the X-axis at a constant speed of 10 m/s (Figure 5). Robustness to the wind disturbances is evaluated by applying wind turbulence and wind gusts of 10 km/h in the $-X$ direction, and 20 km/h in the $-Y$ direction (Figure 5). The specifications in Table II are fulfilled: in presence of wind disturbances, the errors on the trajectory are within ± 1 m on X and Y (Figure 6), and the speed variations are within ± 0.2 m/s (Figure 7). The angles are stabilized which can allow an efficient post-treatment of the acquired radar data (Figure 8). Finally, the control signals are sufficiently smooth and within allowed control amplitudes (Figure 9).

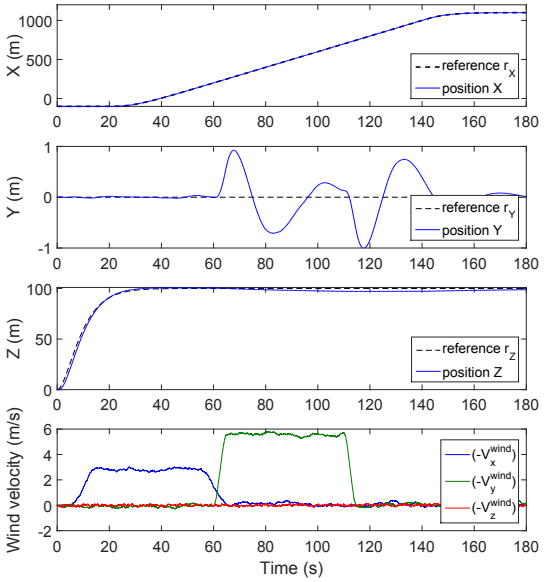

Figure 5: Positions X, Y, Z and wind disturbance profile.

V. Conclusion

In the context of an educational project, this paper proposes an H_∞ control design of an octorotor for radar applications.

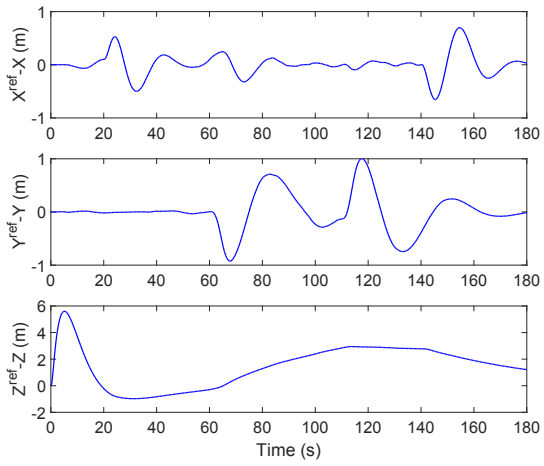

Figure 6: Errors on X, Y, Z.

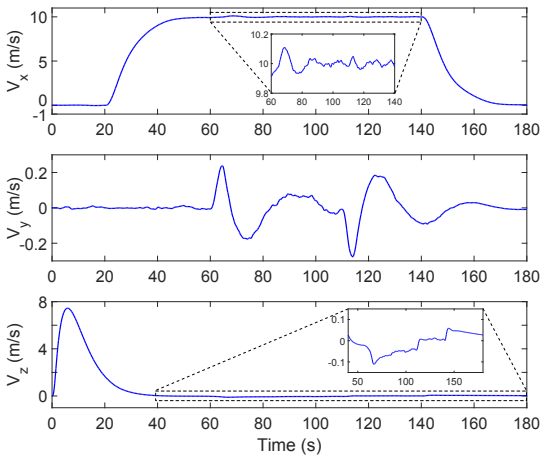

Figure 7: Speeds V_x, V_y, V_z.

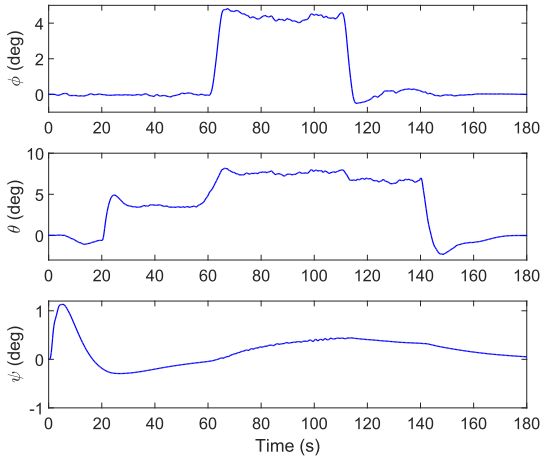

Figure 8: Angles φ, θ, ψ.

A linearized model is used for the controller synthesis. The proposed control law is validated on the complete nonlinear model in a windy scenario. Current work focuses on the comparison with different control laws and on the implementation on the real drone.

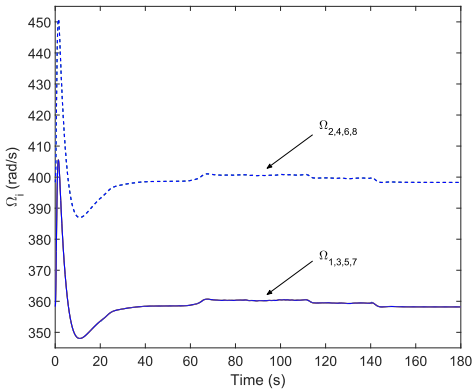

Figure 9: Control inputs - motor speeds Ω_i (odd numbered - solid line, even numbered - dotted line).

ACKNOWLEDGEMENT

The authors would like to thank the students involved in this research and eduational project: Fetra Rasoanarivo, Kodjo Mawonou, and Nicolas Bonnefoy.

REFERENCES

[1] E. C. Zaugg, D. L. Hudson, and D. G. Long, "The BYU SAR: A small, student-built SAR for UAV operation," in *IEEE Int. Conf. on Geoscience and Remote Sensing Symposium*, 2006, pp. 411–414.

[2] J.-T. González-Partida, P. Almorox-González, M. Burgos-García, and B.-P. Dorta-Naranjo, "SAR system for UAV operation with motion error compensation beyond the resolution cell," *Sensors*, vol. 8, no. 5, pp. 3384–3405, 2008.

[3] I. Sa and P. Corke, "System identification, estimation and control for a cost effective open-source quadcopter," in *IEEE Int. Conf. on Robotics and Automation (ICRA)*, 2012, pp. 2202–2209.

[4] K. Bergman and J. Ekström, "Modeling, estimation and attitude control of an octorotor using PID and L1 adaptive control techniques," Master's thesis, Linköping University, Automatic Control, The Institute of Technology, 2014.

[5] M. Makarov, C. Stoica Maniu, S. Tebbani, I. Hinostroza, M. Moreira Beltrami, J. Kienitz, R. Menegazzi, C. Sallé Moreno, T. Rocheron, and J. Rojas Lombarte, "Octorotor UAVs for radar applications: modeling and analysis for control design," in *Workshop on Research, Education and Development of Unmanned Aerial Systems, Cancun, Mexico*, 2015.

[6] I. Sarras and H. Siguerdidjane, "On the guidance of a UAV under unknown wind disturbances," in *IEEE Conf. on Control Applications (CCA)*, 2014, pp. 820–825.

[7] S. Bouabdallah, A. Noth, and R. Siegwart, "PID vs LQ control techniques applied to an indoor micro quadrotor," in *IEEE/RSJ Int. Conf. on Intelligent Robots and Systems (IROS)*, vol. 3, 2004, pp. 2451–2456.

[8] T. Magnusson, "Attitude control of a hexarotor," Master's thesis, Linköping Univ., Automatic Control, The Institute of Technology, 2014.

[9] V. G. Adir and A. M. Stoica, "Integral LQR control of a star-shaped octorotor," *INCAS Bulletin*, vol. 4, no. 2, 2012.

[10] H. Alwi and C. Edwards, "Fault tolerant control of an octorotor using LPV based sliding mode control allocation," in *IEEE American Control Conf. (ACC)*, 2013, pp. 6505–6510.

[11] M.-D. Hua, T. Hamel, P. Morin, and C. Samson, "Introduction to feedback control of underactuated vtolvehicles: A review of basic control design ideas and principles," *Control Systems, IEEE*, vol. 33, no. 1, pp. 61–75, 2013.

[12] L. Li, L. Sun, and J. Jin, "Survey of advances in control algorithms of quadrotor unmanned aerial vehicle," in *16th Int. Conf. on Communication Tech. (ICCT)*. IEEE, 2015, pp. 107–111.

[13] D.-Y. Jeong, T. Kang, H. R. Dharmayanda, and A. Budiyono, "H-infinity attitude control system design for a small-scale autonomous helicopter with nonlinear dynamics and uncertainties," *Journal of aerospace engineering*, vol. 25, no. 4, pp. 501–518, 2011.

[14] S. Kingsley and Q. S., *Understanding Radar Systems*. UK: McGraw-Hill, 1992.